Technical Report

TR-2008-008

A model preconditioner for the Bidomain problem in electrocardiology

by

L. Gerardo-Giorda, L. Mirabella, F. Nobile, M. Perego, A. Veneziani

Mathematics and Computer Science

EMORY UNIVERSITY

A model preconditioner for the Bidomain problem in electrocardiology

L. Gerardo-Giorda

Dep. of Mathematics and Computer Science, Emory University, Atlanta, USA

L. Mirabella *

MOX, Dep. of Mathematics, Politecnico di Milano, Milano, Italy, and
Dep. of Mathematics and Computer Science, Emory University, Atlanta, USA

F. Nobile

MOX, Dep. of Mathematics, Politecnico di Milano, Milano, Italy

M. Perego

MOX, Dep. of Mathematics, Politecnico di Milano, Milano, Italy, and
Dep. of Mathematics and Computer Science, Emory University, Atlanta, USA

A. Veneziani

Dep. of Mathematics and Computer Science, Emory University, Atlanta, USA

Abstract

We introduce a preconditioner for the solution of the Bidomain system governing the propagation of action potentials in the myocardial tissue, represented by a degenerate parabolic set of nonlinear reaction-diffusion equations. The nonlinear term describes the ion flux at the cellular level. The degenerate nature of the problem results in a severe ill conditioning of its discretization. Our preconditioning strategy is based on a suitable adaptation of the Monodomain model, a simplified version of the Bidomain one, which is by far simpler to solve, nevertheless is unable to capture significant features of the action potential propagation. We prove optimality for the preconditioner with respect to the mesh size, and corroborate our results with 3D numerical simulations.

* Corresponding author.
Email addresses: luca@mathcs.emory.edu (L. Gerardo-Giorda),

1 Introduction

The *Bidomain model* is currently considered one of the most complete models for the description of electrical potential in the cardiac tissue (see e.g. [21], [14]). It consists of a system of nonlinear unsteady partial differential equations including the dynamics of intra and extracellular potentials. The degenerate parabolic nature of this system implies high computational costs in the numerical solution. For this reason in many applications a simplified formulation of the problem, called *Monodomain model*, has been preferred. Other studies have been devoted to devise effective preconditioners for the algebraic system obtained after the discretization of the Bidomain model (see e.g. [9], [24], [26], [19],[25]). In general, proposed strategies are based on a proper decomposition of the computational domain for setting up parallel preconditioners, or on suitable multigrid schemes still coupled with parallel architectures.

In this work, we present a different approach, that can be used on serial and on parallel architectures as well and that, at some extent, can be coupled with the techniques mentioned above. As a matter of fact, we propose to *use the Monodomain model*, properly formulated, *as a preconditioner in solving the Bidomain system*. The Monodomain simplification is based on the assumption of proportionality between the intra- and extra-cellular conductivities tensors. This assumption is in general quite unrealistic. However, in this work we show how it succeeds in preconditioning the Bidomain system with optimal performances, i.e. the number of preconditioned iterations results to be independent of the mesh size. This feature is particularly significant in view of 3D simulations on real geometries retrieved by medical data such as SPECT or MRI (see e.g. [6], [3]). Even if resorting to parallel architectures is not mandatory for this strategy, we expect that their adoption could induce a further strong reduction in CPU times.

The outline of the paper is as follows. In Section 2 we introduce the Bidomain and the Monodomain models. In Section 3 we introduce the preconditioned problem and its relevant features. Moreover, we introduce the flexible GMRES (right) preconditioned iterations of the problem at hand. In Section 4 we present an analysis of the preconditioner based on a frequency analysis, similar to the one carried out in [13] and [4] for advection diffusion and Maxwell problems respectively. Our analysis, based on a linearized formulation of the problem stemming from a classical semi-implicit time discretization, shows that the conditioning of the preconditioned problem is bounded by a constant independent of the mesh size h, so that the number of preconditioned iterations

`lucia.mirabella@mail.polimi.it` (L. Mirabella), `fabio.nobile@polimi.it` (F. Nobile), `mauro.perego@polimi.it` (M. Perego), `ale@mathcs.emory.edu` (A. Veneziani).

is expected to be independent of h. Numerical results of Section 5 refer to 3D simulations, carried out with `LifeV` [1], a finite element solver whose linear algebra solver is based on `Trilinos` packages ([2]). More precisely, we present performance comparison between our preconditioner and the algebraic ILU preconditioner. Optimality of the preconditioner is confirmed, the number of iterations being essentially independent of the mesh size. Comparison in terms of CPU time is favorable too.

2 The Bidomain and Monodomain models

Bidomain model The myocardial tissue is composed of elongated cells, the *cardiac fibers*, connected each other by gap junctions and surrounded by an extracellular medium. From a mathematical point of view, this structure can be modeled as a continuum in which the electrical variables are obtained as the average of the single cell properties, after a homogenization process [11]. The cardiac tissue can be represented as a superposition of intra- and extra-cellular media connected by a cell membrane dislocated in the domain. The *Bidomain* model stemming from this approach takes into account the direction of the cardiac fibers. Anatomical studies show that the fibers direction rotates counterclockwise from epicardium to endocardium and that they are arranged in sheets, running across the membrane [9,16]. We set the problem in a bounded region $\Omega \subset \mathbb{R}^3$, and we assume that the cardiac tissue is characterized at each point by three directions: $\boldsymbol{a}_l$ along the fiber, $\boldsymbol{a}_t$ orthogonal to the fiber direction and in the fiber sheet and $\boldsymbol{a}_n$ orthogonal to the sheet. The intra and extracellular media present different conductivity values in each direction. We denote by $\sigma_i^l(\boldsymbol{x})$ (resp. $\sigma_e^l(\boldsymbol{x})$) the intracellular (resp. extracellular) conductivity in $\boldsymbol{a}_l(\boldsymbol{x})$ direction at point $\boldsymbol{x} \in \Omega$, and similarly by $\sigma_i^t(\boldsymbol{x})$ ($\sigma_e^t(\boldsymbol{x})$) and $\sigma_i^n(\boldsymbol{x})$ ($\sigma_e^n(\boldsymbol{x})$) the conductivities along $\boldsymbol{a}_t(\boldsymbol{x})$ and $\boldsymbol{a}_n(\boldsymbol{x})$. We will use the notation $\sigma_{i,e}^l(\boldsymbol{x})$, $\sigma_{i,e}^n(\boldsymbol{x})$, $\sigma_{i,e}^t(\boldsymbol{x})$ for indicating intra and extracellular conductivity in a compact form.

The intra and extracellular local anisotropic conductivity tensors read therefore

$$\mathbf{D}_{i,e}(\boldsymbol{x}) = \sigma_{i,e}^l(\boldsymbol{x})\boldsymbol{a}_l(\boldsymbol{x})\boldsymbol{a}_l^T(\boldsymbol{x}) + \sigma_{i,e}^t(\boldsymbol{x})\boldsymbol{a}_t(\boldsymbol{x})\boldsymbol{a}_t^T(\boldsymbol{x}) + \sigma_{i,e}^n(\boldsymbol{x})\boldsymbol{a}_n(\boldsymbol{x})\boldsymbol{a}_n^T(\boldsymbol{x}). \quad (1)$$

If the myocardium shows the same conductivity in both the tangential and normal direction (*axial isotropy*), the tensors simplify in

$$\mathbf{D}_{i,e}(\boldsymbol{x}) = \sigma_{i,e}^t\mathbf{I} + (\sigma_{i,e}^l - \sigma_{i,e}^t)\boldsymbol{a}_l(\boldsymbol{x})\boldsymbol{a}_l^T(\boldsymbol{x}). \quad (2)$$

In the present work, we assume (2) to hold (see [9]). Moreover, we assume that $\mathbf{D}_{i,e}$ fulfill in Ω a uniform elliptic condition.

Let $u_{i,e}$ be the *intra and extracellular potentials* and $u = u_i - u_e$ be the *transmembrane potential*. The density current in each domain can be computed as $\mathbf{J}_{i,e} = -\mathbf{D}_{i,e}\nabla u_{i,e}$. The net current flux between the intra and the extracellular domain is assumed to be zero as a consequence of the charge conservation in an arbitrary portion of tissue. Let us denote by I_m the ingoing membrane current flow and by χ the ratio of membrane area per tissue volume. We get therefore

$$\nabla \cdot (\mathbf{D}_i \nabla u_i) \;=\; \chi I_m \;=\; -\nabla \cdot (\mathbf{D}_e \nabla u_e) \tag{3}$$

where $I_m = C_m du/dt + I_{ion}$ being C_m a capacitance and I_{ion} the ionic current. The dependence of I_{ion} on u has been described basically in two different ways in the literature. One approach is based on a precise description of ionic channels like in the models proposed in [5] and [27], and, in particular, the Luo-Rudy phase I model [17]. The second approach is based on a phenomenological evidence. We mention in particular the Fitzhugh-Nagumo [12] and the Rogers-McCulloch [20] models. Our present proposal does not rely on a specific selection of ionic model, so we do not dwell here upon this topic. Numerical results presented hereafter will refer to both the Luo-Rudy phase I and the Rogers-McCulloch models as well.

The complete Bidomain model reads

$$\chi C_m \begin{bmatrix} 1 & -1 \\ -1 & 1 \end{bmatrix} \frac{\partial}{\partial t} \begin{bmatrix} u_i \\ u_e \end{bmatrix} - \begin{bmatrix} \nabla \cdot \mathbf{D}_i \nabla u_i \\ \nabla \cdot \mathbf{D}_e \nabla u_e \end{bmatrix} + \chi \begin{bmatrix} I_{\text{ion}}(u) \\ -I_{\text{ion}}(u) \end{bmatrix} = \begin{bmatrix} I_i^{\text{app}} \\ -I_e^{\text{app}} \end{bmatrix} \tag{4}$$

where I_{ion} depends on the chosen ionic model, and $I_{i,e}^{\text{app}}$ are applied external stimuli. The problem is completed by an initial condition

$$u(\boldsymbol{x}, 0) = u_0 \tag{5}$$

and boundary conditions on $\partial\Omega$. In particular we prescribe homogeneous Neumann boundary conditions

$$\mathbf{n}^T \mathbf{D}_i \nabla u_i(\boldsymbol{x}, t) = 0 \quad \text{and} \quad \mathbf{n}^T \mathbf{D}_e \nabla u_e(\boldsymbol{x}, t) = 0, \quad \text{on } \partial\Omega \times (0, T) \tag{6}$$

where $\mathbf{n}$ is the unit normal outward-pointing vector on the surface, corresponding to an insulated myocardium. As a consequence of the Gauss theorem, the applied external stimuli must fulfill the compatibility condition

$$\int_\Omega I_i^{\text{app}}\, d\boldsymbol{x} = \int_\Omega I_e^{\text{app}}\, d\boldsymbol{x}. \tag{7}$$

System (4) consists of of two parabolic reaction diffusion equations for u_i and u_e where the vector of time derivatives is multiplied by a singular matrix. The system is thus said to be *degenerate*. The transmembrane potential u is uniquely determined, while the intra and extracellular potentials u_i and

u_e are determined up to the same function of time, whose value is usually obtained by imposing that u_e has zero average on Ω. Let us define $\boldsymbol{V} = H^1(\Omega) \times H^1(\Omega)/\{(c,c) : c \in \mathbb{R}\}$ and denote by $(\cdot,\cdot)$ the scalar product in L^2. The variational form of the Bidomain problem reads as follows: given $I_{i,e}^{\text{app}}$ and I_{ion}, find $(u_i, u_e) \in \boldsymbol{V}$ such that

$$\chi C_m(\frac{\partial u}{\partial t}, \phi) + a_i(u_i, \phi_i) + a_e(u_e, \phi_e) + (I_{\text{ion}}, \phi) = (I_i^{\text{app}}, \phi_i) + (I_e^{\text{app}}, \phi_e) \quad (8)$$

for each $(\phi_i, \phi_e) \in \boldsymbol{V}$, where $\phi = \phi_i - \phi_e$. The forms $a_{i,e}(v, \phi)$ are defined as $a_{i,e}(v, \phi) = \int_\Omega \nabla v^T D_{i,e} \nabla \phi \, d\boldsymbol{x}$. For well-posedness analysis of the Bidomain problem coupled with the Fitzhugh-Nagumo ionic model, we refer to [11].

Monodomain model To overcome high computational costs associated with the Bidomain problem a simplified model has been proposed, the so called *Monodomain* problem. Its derivation can be obtained in two different ways. One way consists in assuming $\mathbf{D}_e = \lambda \mathbf{D}_i$, where λ is a constant to be properly chosen. For instance, under assumption (2), one can minimize the functional

$$J = (\sigma_l^e - \lambda \sigma_l^i)^2 + 2\,(\sigma_t^e - \lambda \sigma_i^t)^2$$

for given values of the conductivities. Another way of choosing λ has been proposed in [18]. In general, if we define

$$\lambda_m = \min\left\{ \frac{\sigma_e^l}{\sigma_i^l}\,,\, \frac{\sigma_e^t}{\sigma_i^t} \right\} \qquad \lambda_M = \max\left\{ \frac{\sigma_e^l}{\sigma_i^l}\,,\, \frac{\sigma_e^t}{\sigma_i^t} \right\}, \quad (9)$$

it is reasonable to choose $\lambda_m \le \lambda \le \lambda_M$. Thanks to this assumption, a linear combination of the Bidomain equations with coefficients $\dfrac{\lambda}{1+\lambda}$ and $-\dfrac{1}{1+\lambda}$ yields the Monodomain model

$$\begin{cases} \chi C_m \dfrac{\partial u}{\partial t} - \nabla \cdot (\mathbf{D}^M \nabla u) + \chi I_{\text{ion}} = I^{\text{app}} & \text{in } \Omega \times (0,T) \\ u(\boldsymbol{x}, t=0) = u_0 & \text{in } \Omega \\ \mathbf{n}^T \mathbf{D}^M \nabla u = 0 & \text{on } \partial\Omega \times (0,T), \end{cases} \quad (10)$$

where $\mathbf{D}^M = \dfrac{\lambda \mathbf{D}_i}{1+\lambda}$ e $I^{\text{app}} = \dfrac{\lambda I_i^{\text{app}} + I_e^{\text{app}}}{1+\lambda}$.
Another way to derive a Monodomain model, that we will not use in what follows, can be found in [15] and [7], where the authors mediate the contribution of the intra and extracellular medium. by choosing in (10)

$$\mathbf{D}^M := \mathbf{D}_e\,(\mathbf{D}_i + \mathbf{D}_e)^{-1}\,\mathbf{D}_i, \quad (11)$$

In the sequel we will refer basically to (9), even if the preconditioner proposed can be extended to the problem obtained with (11).

Using the notation introduced in the previous Section, the variational form of the Monodomain problem reads: given I^{app} and I_{ion}, find $u \in H^1(\Omega)$ such that

$$\chi C_m(\frac{\partial u}{\partial t}, \phi) + a_M(u, \phi) + (I_{\text{ion}}, \phi) = (I^{\text{app}}, \phi) \tag{12}$$

for each $\phi \in H^1(\Omega)$. The form $a_M(v, \phi) := \int_\Omega \nabla v^T \mathbf{D}^M \nabla \phi d\boldsymbol{x}$ is bilinear, continuous and weakly coercive on $H^1(\Omega) \times H^1(\Omega)$. For well-posedness analysis of this problem, we still refer to [11].

Monodomain model is a single parabolic reaction-diffusion PDE for the transmembrane potential, replacing the two equations of the original model. However, this model is not able to capture some physiological and pathological patterns of the action potential propagation (see [8]).

3 The preconditioned Bidomain model

As a consequence of the degenerate nature of the Bidomain model that entails a severe ill conditioning of the matrix associated to its fully discrete approximation, the numerical solution of (4) requires a high computational effort. On the contrary, though relying on assumptions that prove quite often to be unrealistic, system (10) is by far more affordable. Our approach now is to use the Monodomain model as a preconditioner for the Bidomain system. To this aim we properly reformulate both systems. More precisely, we consider the non-symmetric form of the Bidomain problem in terms of the transmembrane and the extracellular potentials u and u_e

$$\begin{cases} \chi C_m \dfrac{\partial u}{\partial t} - \nabla \cdot \left(\dfrac{\lambda \mathbf{D}_i}{1+\lambda} \nabla u \right) - \nabla \cdot \left(\dfrac{\lambda \mathbf{D}_i - \mathbf{D}_e}{1+\lambda} \nabla u_e \right) + \chi I_{ion} = I^{\text{app}} \\ -\nabla \cdot [\mathbf{D}_i \nabla u + (\mathbf{D}_i + \mathbf{D}_e) \nabla u_e] = \widetilde{I}^{\text{app}}. \end{cases} \tag{13}$$

This formulation stems from linear combinations of the two equations in (4), with coefficients $(\frac{\lambda}{1+\lambda}, -\frac{1}{1+\lambda})$ and $(1, 1)$, respectively, where we have set $I^{\text{app}} = \dfrac{\lambda I_i^{\text{app}} + I_e^{\text{app}}}{1+\lambda}$ and $\widetilde{I}^{\text{app}} = I_i^{\text{app}} - I_e^{\text{app}}$. In order to match the dimension of the Bidomain problem, Monodomain model needs to be extended. The same linear combination leading to (13), combined with the assumption $\mathbf{D}_e = \lambda \mathbf{D}_i$ yields

the extended Monodomain formulation in terms of the variables u and u_e

$$\begin{cases} \chi C_m \dfrac{\partial u}{\partial t} - \nabla \cdot \left(\dfrac{\lambda \mathbf{D}_i}{1+\lambda} \nabla u \right) + \chi I_{ion} = I^{\text{app}} \\ -\nabla \cdot [\mathbf{D}_i \nabla u + (1+\lambda)\mathbf{D}_i \nabla u_e] = \widetilde{I}^{\text{app}}. \end{cases} \tag{14}$$

System (14) is lower triangular, where the first equation (the "genuine" Monodomain model) is independent of u_e. In view of its use as a preconditioner, however, there is no reason for retaining the simplifying Monodomain assumption $\lambda \mathbf{D}_i = \mathbf{D}_e$ in the second equation so we finally resort to

$$\begin{cases} \chi C_m \dfrac{\partial u}{\partial t} - \nabla \cdot \left(\dfrac{\lambda \mathbf{D}_i}{1+\lambda} \nabla u \right) + \chi I_{ion} = I^{\text{app}} \\ -\nabla \cdot [\mathbf{D}_i \nabla u + (\mathbf{D}_i + \mathbf{D}_e)\nabla u_e] = \widetilde{I}^{\text{app}}. \end{cases} \tag{15}$$

3.1 Numerical discretization

Let Δt be the time step of the discretization, we denote with superscript n the variables computed at time $t^n = n\Delta t$. Moving from time step t^n to t^{n+1} the semi-implicit time discrete Bidomain problem 13 reads

$$\begin{cases} \chi C_m \dfrac{u^{n+1} - u^n}{\Delta t} - \nabla \cdot \left(\dfrac{\lambda \mathbf{D}_i}{1+\lambda} \nabla u^{n+1} + \dfrac{\lambda \mathbf{D}_i - \mathbf{D}_e}{1+\lambda} \nabla u_e^{n+1} \right) = I(u^n) \\ -\nabla \cdot [\mathbf{D}_i \nabla u^{n+1} + (\mathbf{D}_i + \mathbf{D}_e)\nabla u_e^{n+1}] = \widetilde{I}^{\text{app}} \\ u^0(\boldsymbol{x}) = u_0(\boldsymbol{x}) \\ \mathbf{n}^T \mathbf{D}_i (\nabla u^{n+1} + \nabla u_e^{n+1}) = 0 \qquad \mathbf{n}^T \mathbf{D}_e \nabla u_e^{n+1} = 0 \end{cases} \tag{16}$$

where we have set $I(u^n) = I^{\text{app}} - \chi I_{ion}(u^n)$, the latter term including the selected model for ionic current. Concerning the spatial approximation, we discretize the domain Ω with a triangulation $\mathcal{T}_h$ and we build a finite element space V_h approximating V on $\mathcal{T}_h$, in which we will look for the approximate solution u^h and u_e^h. In this work V_h is the space of piecewise linear continuous functions on $\mathcal{T}_h$, and we denote by $\Phi = \{\varphi_j\}_{j=1}^{N_h}$ a basis for V_h. Well-posedness of the discrete problem and convergence analysis for the Rogers-McCulloch model are carried out in [23].
Let us denote by $\mathcal{M}$ the mass matrix with entries $\mathcal{M}^{ij} = \sum_{K \in \mathcal{T}_h} (\varphi_j, \varphi_i)|_K$, and by $\mathcal{K}_{i,e}$ the stiffness matrices with $\mathcal{K}_{i,e}^{ij} = \sum_{K \in \mathcal{T}_h} (\mathbf{D}_{i,e} \nabla \varphi_j, \nabla \varphi_i)|_K$, $\varphi_i,\ \varphi_j \in \Phi$. The unknowns of the fully discrete problem are represented by vectors $\mathbf{u}$ and $\mathbf{u}_e$, storing the nodal values of u^h and u_e^h, respectively, we let $\mathbf{f}$ and $\mathbf{g}$ denote

the discretization of the forcing terms, and we set

$$\mathbf{B}_{uu} = \frac{\mathcal{M}}{\Delta t} + \frac{\lambda \mathcal{K}_i}{1+\lambda} \quad \mathbf{B}_{ue} = \frac{\lambda \mathcal{K}_i}{1+\lambda} - \frac{\mathcal{K}_e}{1+\lambda} \quad \mathbf{B}_{eu} = \mathcal{K}_i \quad \mathbf{B}_{ee} = \mathcal{K}_i + \mathcal{K}_e.$$

At step t^{n+1} we solve

$$\mathbf{B}_{\mathrm{NS}} \mathbf{u}_{\mathrm{NS}}^{n+1} = \mathbf{f}_{\mathrm{NS}}^{n}, \tag{17}$$

where

$$\mathbf{B}_{\mathrm{NS}} = \begin{bmatrix} \mathbf{B}_{uu} & \mathbf{B}_{ue} \\ \mathbf{B}_{eu} & \mathbf{B}_{ee} \end{bmatrix}, \qquad \mathbf{u}_{\mathrm{NS}} = \begin{bmatrix} \mathbf{u} \\ \mathbf{u}_e \end{bmatrix}, \qquad \mathbf{f}_{\mathrm{NS}} = \begin{bmatrix} \mathbf{f} \\ \mathbf{g} \end{bmatrix}.$$

As a preconditioner for (17) we select

$$\mathbf{M}_{\mathrm{NS}} = \begin{bmatrix} \mathbf{B}_{uu} & \mathbf{0} \\ \mathbf{B}_{eu} & \mathbf{B}_{ee} \end{bmatrix}.$$

Notice that in this form model preconditioner based on the Monodomain model can be interpreted at the discrete level as a Gauss-Seidel preconditioner on the non symmetric formulation of the Bidomain problem in terms of u and u_e. The interpretation of the preconditioner as a consequence of extension of the Monodomain model has however some advantages in view of devising a domain decomposition multi-model solver for $u_{i,e}$, that will be addressed in a forthcoming paper.
In principle, the same approach based on the block-triangular preconditioning could be applied also to the symmetric formulation of the Bidomain system in terms of u_i and u_e. However, this choice proves to be uneffective, as we show in Section 5.

Since matrix in (17) is not symmetric, system has to be solved by a Krylov type method. If the linear system associated with the preconditioner is solved once for all (for instance with an ILU factorization) one can use a preconditioned GMRES (see [22]) to solve (17), without further considerations on the kind of preconditioning (left or right). On the other hand, when the preconditioning matrix is obtained at each time step by solving the Monodomain system via an iterative method, the preconditioner changes at each iteration, and one has to use a flexible GMRES (FGMRES), which demands right preconditioning ([22]).
The implementation of FGMRES requires to solve system $\mathbf{M}_{\mathrm{NS}}\mathbf{z} = \mathbf{v}$, where $\mathbf{z} = [\mathbf{z}^1, \mathbf{z}^2]^T$ and $\mathbf{v} = [\mathbf{v}^1, \mathbf{v}^2]^T$. To this aim, we exploit the lower triangular structure of $\mathbf{M}_{\mathrm{NS}}$, solving

$$\mathbf{B}_{uu}\mathbf{z}^1 = \mathbf{v}^1 \qquad \mathbf{b} = \mathbf{v}^2 - \mathbf{B}_{eu}\mathbf{z}^1 \qquad \mathbf{B}_{ee}\mathbf{z}^2 = \mathbf{b}. \tag{18}$$

Using FGMRES allows to solve systems (18) with a coarse tolerance, for the sake of CPU time reduction, as we will illustrate later on.

4 Fourier analysis of the preconditioner

In this section we analyze the performances of the proposed preconditioner at each time step by means of Fourier analysis. For the sake of clarity, we drop hereafter the time index. We assume, without loss of generality, the reference frame to have the first component aligned with the longitudinal axis of the fibers, so that, owing to (2), the diffusion tensors are diagonal. We introduce the continuous opertors $\mathcal{B} : [H^1(\Omega)]^2 \to [H^{-1}(\Omega)]^2$ and $\mathcal{M} : [H^1(\Omega)]^2 \to [H^{-1}(\Omega)]^2$, associated with problems (16) and with the semi-discrete counterpart of (15). Denoting by k_1, k_2 and k_3 the dual variables, the Fourier transform of $w(x, y, z) = u(x, y, z), u_e(x, y, z)$ reads

$$\mathcal{F} : w(x, y, z) \mapsto \widehat{w}(k_1, k_2, k_3) = \int\int\int_{\mathbb{R}^3} e^{-i(k_1 x + k_2 y + k_3 z)} w(x, y, z)\, dxdydz,$$

and the action of the operators $\mathcal{B}$ and $\mathcal{M}$ can be expressed for any $u \in [H^1(\Omega)]^2$ as

$$\mathcal{B}u = \mathcal{F}^{-1}\left(B\widehat{u}\right) \qquad\qquad \mathcal{M}u = \mathcal{F}^{-1}\left(M\widehat{u}\right)$$

where B and M represent the operators $\mathcal{B}$ and $\mathcal{M}$, respectively. We denote by $(f, g)^T$ the right hand side in (16), and, owing to assumption (2), we let $\boldsymbol{k}^2 = k_2^2 + k_3^2$. The transformed (linearized) Bidomain problem reads

$$\begin{aligned} &\chi C_m \widehat{u} + \frac{\Delta t}{1+\lambda}\left(\lambda\left[\sigma_i^l k_1^2 + \sigma_i^t \boldsymbol{k}^2\right]\widehat{u} + \left[(\lambda\sigma_i^l - \sigma_e^l)k_1^2 + (\lambda\sigma_i^t - \sigma_e^t)\boldsymbol{k}^2\right]\widehat{u}_e\right) = \widehat{f} \\ &\left[\sigma_i^l k_1^2 + \sigma_i^t \boldsymbol{k}^2\right]\widehat{u} + \left[(\sigma_i^l + \sigma_e^l)k_1^2 + (\sigma_i^t + \sigma_e^t)\boldsymbol{k}^2\right]\widehat{u}_e = \widehat{g}. \end{aligned} \tag{19}$$

The first equation of the expanded Monodomain problem reads

$$\chi C_m \widehat{u} + \Delta t \frac{\lambda}{1+\lambda}\left[\sigma_i^l k_1^2 + \sigma_i^t \boldsymbol{k}^2\right]\widehat{u} = \widehat{f},$$

the second transformed equation coinciding with the second equation in (19). We set $\xi = \sigma_i^l k_1^2 + \sigma_i^t \boldsymbol{k}^2$, and $\eta = \sigma_e^l k_1^2 + \sigma_e^t \boldsymbol{k}^2$. Bidomain and Monodomain problems in the frequency domain can be rewritten in matrix form as

$$B(k_1, \boldsymbol{k}) \begin{bmatrix} \widehat{u} \\ \widehat{u}_e \end{bmatrix} = \begin{bmatrix} \widehat{f} \\ \widehat{g} \end{bmatrix} \qquad\qquad M(k_1, \boldsymbol{k}) \begin{bmatrix} \widehat{u} \\ \widehat{u}_e \end{bmatrix} = \begin{bmatrix} \widehat{f} \\ \widehat{g} \end{bmatrix}$$

where

$$B(k_1,\boldsymbol{k}) = \begin{bmatrix} \chi C_m + \Delta t \frac{\lambda}{1+\lambda}\,\xi(k_1,\boldsymbol{k}) & \Delta t\left[\frac{\lambda}{1+\lambda}\,\xi(k_1,\boldsymbol{k}) - \frac{1}{1+\lambda}\,\eta(k_1,\boldsymbol{k})\right] \\ \\ \xi(k_1,\boldsymbol{k}) & \xi(k_1,\boldsymbol{k}) + \eta(k_1,\boldsymbol{k}) \end{bmatrix} \tag{20}$$

and

$$M(k_1,\boldsymbol{k}) = \begin{bmatrix} \chi C_m + \Delta t \frac{\lambda}{1+\lambda}\,\xi(k_1,\boldsymbol{k}) & 0 \\ \\ \eta(k_1,\boldsymbol{k}) & \xi(k_1,\boldsymbol{k}) + \eta(k_1,\boldsymbol{k}) \end{bmatrix}. \tag{21}$$

For $(k_1,\boldsymbol{k}) \neq (0,0)$ the matrix $M(k_1,\boldsymbol{k})$ is invertible and the preconditioned problem in the frequency domain reads

$$[M(k_1,\boldsymbol{k})]^{-1}\, B(k_1,\boldsymbol{k})\, (\widehat{u},\widehat{u}_e)^T = [M(k_1,\boldsymbol{k})]^{-1}\, (\widehat{f},\widehat{g})^T.$$

From now on we set $\chi C_m = 1$, as this is the standard assumption in the applications (see [10]).
Considering $|k_1| < k_1^M$ and $|\boldsymbol{k}| < \boldsymbol{k}^M$, we analyze the effectiveness of the preconditioned operator over the domain

$$T = \{\lambda_M\xi - c_1 \leq \eta \leq \lambda_M\xi,\ \lambda_m\xi \leq \eta \leq \lambda_m\xi + c_2\} \setminus \{(0,0)\},$$

shown in Figure 1, where c_1 and c_2 are positive constants depending on $k_1^M, \boldsymbol{k}^M$ and on the conductivity values. As k_1^M and $\boldsymbol{k}^M$ tend to infinity, the domain T covers the angular sector $S = \{\lambda_m\xi \leq \eta \leq \lambda_M\xi\} \setminus \{(0,0)\}$.

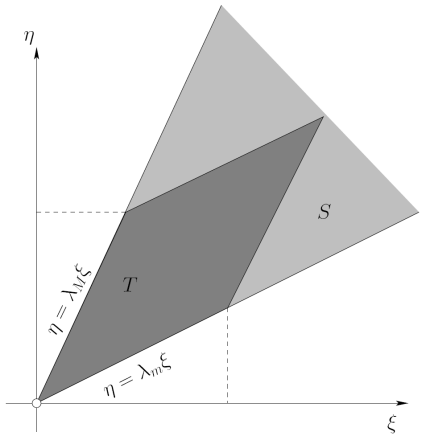

Figure 1. The domains T and S.

With these notations, the preconditioned operator reads

$$[M(\xi,\eta)]^{-1}\,B(\xi,\eta) = \begin{bmatrix} 1 & \alpha(\xi,\eta) \\ 0 & 1-\dfrac{\xi}{\xi+\eta}\alpha(\xi,\eta) \end{bmatrix}, \tag{22}$$

where

$$\alpha(\xi,\eta) = \frac{\Delta t}{1+\lambda}\,\frac{[\lambda\,\xi-\,\eta]}{1+\frac{\lambda}{1+\lambda}\,\Delta t\,\xi}. \tag{23}$$

Notice that, for $\Delta t \to 0$, the preconditioning tends to be exact, as the matrix in (22) tends to the identity.
The eigenvalues of $M^{-1}B$ are clearly given by

$$\gamma_1(\xi,\eta) = 1 \qquad \gamma_2(\xi,\eta) = 1-\frac{\xi}{\xi+\eta}\alpha(\xi,\eta) = \frac{1+\Delta t\xi\,\dfrac{1}{\frac{\xi}{\eta}+1}}{1+\Delta t\xi\,\dfrac{1}{\frac{1}{\lambda}+1}}. \tag{24}$$

Since they are both real and positive, the conditioning of the continuous preconditioned problem is estimated by the ratio between their maximum and their minimum. From (23), we have $\gamma_2(\xi,\eta) < 1$ for $\eta < \lambda\xi$ and $\gamma_2(\xi,\eta) > 1$ for $\eta > \lambda\xi$, thus, for any $\lambda_m \le \lambda \le \lambda_M$

$$\mathcal{K}\left(\mathcal{M}^{-1}\mathcal{B}\right) = \frac{\max\left[1,\,\max\limits_{(\xi,\eta)\in T}\gamma_2(\xi,\eta)\right]}{\min\left[1,\,\min\limits_{(\xi,\eta)\in T}\gamma_2(\xi,\eta)\right]} = \frac{\max\limits_{(\xi,\eta)\in T}\gamma_2(\xi,\eta)}{\min\limits_{(\xi,\eta)\in T}\gamma_2(\xi,\eta)}. \tag{25}$$

Since $\frac{1}{\lambda_M} \le \frac{\xi}{\eta} \le \frac{1}{\lambda_m}$, we have

$$\Gamma_m(\xi) = \frac{1+\Delta t\xi\,\dfrac{1}{\frac{1}{\lambda_m}+1}}{1+\Delta t\xi\,\dfrac{1}{\frac{1}{\lambda}+1}} \le \gamma_2(\xi,\eta) \le \frac{1+\Delta t\xi\,\dfrac{1}{\frac{1}{\lambda_M}+1}}{1+\Delta t\xi\,\dfrac{1}{\frac{1}{\lambda}+1}} = \Gamma_M(\xi), \tag{26}$$

namely, $\gamma_2(\xi,\eta)$ is bounded independently of η. For any $\lambda_m \le \lambda \le \lambda_M$, $\Gamma_m(\xi)$ is nonincreasing and $\Gamma_M(\xi)$ is nondecreasing. Taking the limit for $\xi,\,\eta \to \infty$ in (26), corresponding to $h \to 0$, domain T does coincide with S and we get

$$\min_{(\xi,\eta)\in T}\gamma_2(\xi,\eta) \ge \frac{\frac{1}{\lambda}+1}{\frac{1}{\lambda_m}+1} \qquad \max_{(\xi,\eta)\in T}\gamma_2(\xi,\eta) \le \frac{\frac{1}{\lambda}+1}{\frac{1}{\lambda_M}+1}. \tag{27}$$

Gathering together (25) and (27) we obtain that for all $\lambda_m \leq \lambda \leq \lambda_M$

$$\mathcal{K}\left(\mathcal{M}^{-1}\mathcal{B}\right) \leq \left(1+\frac{1}{\lambda_M}\right)^{-1}\left(1+\frac{1}{\lambda_m}\right). \tag{28}$$

We conclude that the preconditioner is optimal with respect to the mesh size, since the stability of the continuous problem $\mathcal{K}\left(\mathcal{M}^{-1}\mathcal{B}\right)$ is bounded by a constant depending only on the anisotropy ratio in the coefficients of the Bidomain problem.
The previous analysis suggests some further considerations on λ. Beyond physical considerations, λ can be considered here as a parameter to be selected for enhancing the convergence of the preconditioned iterations. We plot in Figure 2 the distribution of the generalized eigenvalues ω of the matrices $\mathbf{B}_{\mathrm{NS}}$ and $\mathbf{M}_{\mathrm{NS}}$ ($\mathbf{B}_{\mathrm{NS}}\boldsymbol{v} = \omega\,\mathbf{M}_{\mathrm{NS}}\boldsymbol{v}$), computed with Matlab®, for two different mesh sizes and for $\lambda = \lambda_m$, $\lambda = \lambda_M$, and $\lambda = 1.3$, which is the value used in the numerical simulations of Sect. 5. As expected from the Fourier analysis, all the eigenvalues are greater than 1 for $\lambda = \lambda_m$, and smaller than 1 for $\lambda = \lambda_M$ indipendently of the mesh size. Notice that the spectrum spreads out as the mesh parameter h decreases. The choice of $\lambda = 1.3$, empirically driven for minimizing computational costs, leads to a good clustering of the spectrum around 1.

5 Numerical results

Numerical results presented hereafter refer to the 3D Bidomain problem set on a truncated ellipsoid, representing a simplified ventricular geometry, and on a slab. Both these geometries are completed with an analytical representation of the fiber orientation as detailed in [9]. In the truncated ellipsoid simulation the Bidomain model is coupled both with the Rogers-McCulloch and the Luo-Rudy Phase I ionic models, while the simulation on the slab refers to the Luo-Rudy Phase I model. In our numerical tests we consider the parameters listed in [17] for the Luo-Rudy ionic model and the parameters in [9] to set the Rogers-McCulloch model and the Bidomain one.
The performances of our preconditioner applied to the non symmetric formulation of the Bidomain problem, and solved via a flexible GMRES algorithm (FGMRES), are compared with a ILU preconditioned conjugate gradient (PCG) applied to the symmetric Bidomain formulation. The latter at each time t^{n+1} reads

$$\mathbf{B}_{\mathrm{S}}\ \mathbf{u}_{\mathrm{S}}^{n+1} = \mathbf{f}_{\mathrm{S}}^{n} \tag{29}$$

where

$$\mathbf{B}_{\mathrm{S}} = \begin{bmatrix} \mathbf{B}_{ii}^{S}\ \mathbf{B}_{ie}^{S} \\ \mathbf{B}_{ei}^{S}\ \mathbf{B}_{ee}^{S} \end{bmatrix}, \qquad \mathbf{u}_{\mathrm{S}} = \begin{bmatrix} \mathbf{u}_i \\ \mathbf{u}_e \end{bmatrix}, \qquad \mathbf{f}_{\mathrm{S}} = \begin{bmatrix} \mathbf{f}_i \\ \mathbf{f}_e \end{bmatrix}$$

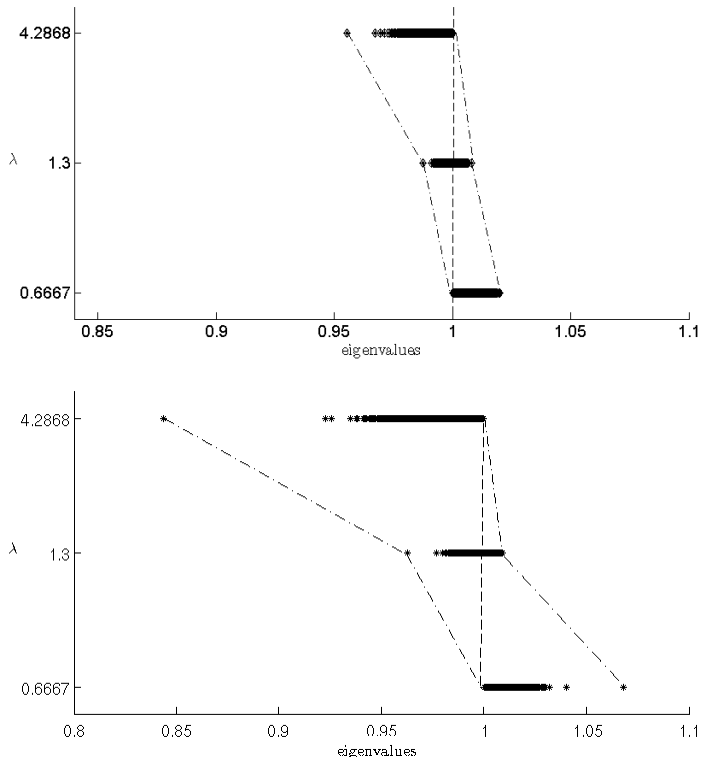

Figure 2. Spectra of the preconditioned problem for different mesh sizes: 5272 nodes (left) and 12586 nodes (right). The dashed-dotted lines highlight clustering of the eigenvalues around 1 for different values of λ.

and

$$\mathbf{B}_{ii}^S = \frac{\mathcal{M}}{\Delta t} + \mathcal{K}_i, \qquad \mathbf{B}_{ie}^S = \mathbf{B}_{ei}^S = -\frac{\mathcal{M}}{\Delta t}, \qquad \mathbf{B}_{ee}^S = \frac{\mathcal{M}}{\Delta t} + \mathcal{K}_e.$$

Entries of vectors $\mathbf{u}_i$ and $\mathbf{u}_e$ are the nodal values of u_i^h and u_e^h, while vectors $\mathbf{f}_i$ and $\mathbf{f}_e$ represent the discretization of the forcing terms in the two equations.

Numerical simulation are carried out with `LifeV` ([1]), a finite element based code that uses `Trilinos` packages ([2]) to solve the linear systems: system (29) is solved by a Block-CG algorithm implemented in `BELOS` package, with an ILU left preconditioner (with drop tolerance 10^{-9} and level of fill 1), implemented in `Ifpack` package, while system (17) is solved by a Flexible Block-GMRES implemented in `BELOS`. Finally, both linear systems in (18) are symmetric and are solved by a Block-CG with an ILU left preconditioner. All the computations are carried out on a workstation equipped with a 2.2 GHz AMD Dual-Core Opteron processor and 4 GB RAM.

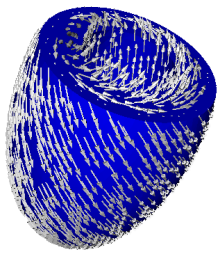

Figure 3. Truncated ellipsoidal geometry representing a left ventricle. White arrows represent myocardial fiber orientation used in our numerical simulations (see [9] for their analytical description).

5.1 Influence of the inner tolerance

The first set of numerical experiments aims at investigating the robustness of the preconditioner with respect to the accuracy in the solution of systems (18). We performed numerical simulation over an idealized ventricular geometry represented by the truncated ellipsoid reported in Figure 3.

We set $\lambda = 1.3$, $\Delta t = 0.1$ ms, and the simulation is run for 50 ms with the Luo-Rudy phase I model. We solve here systems (18) with a tolerance $toll = 10^{-5}$, which is the same tolerance used as a stopping criterion in the outer iterations. Then we solved the same problem with a coarse tolerance $tol = 0.12$ for solving systems (18), which is the result of a fine tuning for finding a trade-off between the number of outer iterations and CPU time to solve (18). The stopping criterion for the solution of all the linear systems mentioned is based on the control of 2-norm of the current residual, normalized respect to the 2-norm of the initial residual.

In Table 1 we report the average CPU time and the average FGMRES iteration counts over the entire simulation with different mesh sizes. The two solutions of the Bidomain systems are computed up to the fulfillment of the same outer tolerance on the residual. Table 1 highlights the relevant CPU time reduction with the use of a coarse inner tolerance, while the outer iteration counts are almost insensitive to the different accuracy required to the solution of the preconditioning systems.

5.2 Long time simulation

In this test we analyze the effectiveness of the Monodomain preconditioner on an entire action potential duration (APD), namely for 400 ms on a fine grid.

	$tol = 10^{-5}$		$tol = 0.12$	
# nodes	avg. time	# iter	avg. time	# iter
29560	3.89158	2.988	1.08365	3.068
62566	10.6337	3	3.82078	3.972
172878	53.0898	3.922	15.4344	3.99

Table 1
Comparison of the performances of the preconditioner with a fine vs coarse inner resolution.

In particular we choose $h = 0.02$ cm on a computational domain given by a slab geometry of size 1x1x0.2 cm, that can be handled on a single processor computer. The resulting tetrahedral grid counts 208848 points.

Bidomain system is coupled with the Luo-Rudy Phase I model. We set again $\Delta t = 0.1$ ms, $\lambda = 1.3$, and we solve the systems in (18) with an inner tolerance $toll = 0.12$, while the outer tolerance is 10^{-5}. We plot in Figure 4 (top) the evolution of the iteration counts for both the ILU preconditioned problem and the Monodomain preconditioned problem (denoted *MPrec*). ILU preconditioner simulation shows a remarkable variation in the iteration counts at the beginning and at the end of the simulation, as already observed in [24]. Correspondingly, CPU time at the beginning and at the end of simulation is increased. This is likely a consequence of large variations in the ionic current (due to the upstroke propagation and to the closing of gating channels), occurring at the beginning and the end of APD, that are amplified by the ill conditioning of the Bidomain problem. On the other hand the Monodomain preconditioner has a constant performance along the whole simulation in terms of the number of iterations at each time step, which is remarkably smaller than in the ILU preconditioner case. CPU time plot (Figure 4, bottom) shows that, also for our preconditioner, the CPU time slightly increases, as to be expected still for the large variations of the ionic current. This effect is however by far less evident for our preconditioner versus the ILU one.

5.3 Influence of the mesh size

In the last test we run the Bidomain simulation on the truncated ellipsoid for 50 ms. In the coupling with the Rogers-McCulloch model the time step used is $\Delta t = 0.5$ ms, while with the Luo-Rudy Phase I model $\Delta t = 0.1$ ms is required, in order to solve the ionic current problem accurately enough. We set again $\lambda = 1.3$. The tolerance for systems (18) is $tol = 0.12$, while the tolerance for the outer iterations is set at 10^{-5} for both the Flexible GMRES and the PCG. We compare the iteration counts and the execution time of the Bidomain

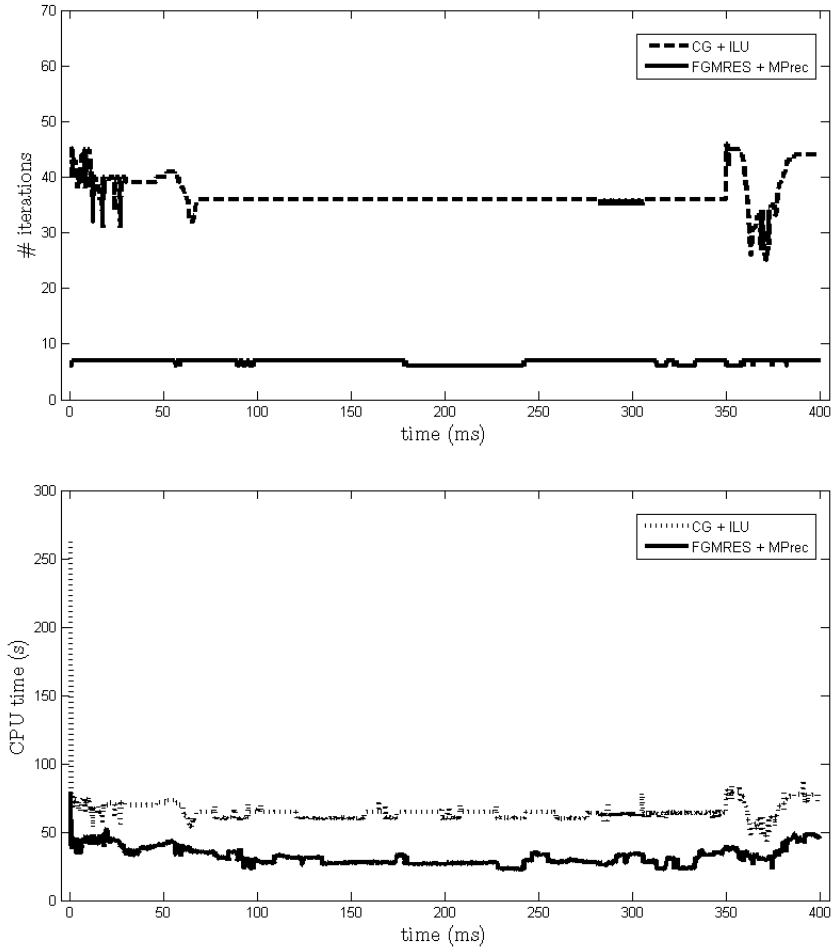

Figure 4. Test of section 5.2: top: number of iterations at each time step. In dashed line: conjugate gradient method with ILU preconditioner; in solid line: flexible GMRES with Monodomain preconditioner. Bottom: CPU time for the solution of the linear system at each time step. In dotted line: conjugate gradient method with ILU preconditioner; in solid line: flexible GMRES with Monodomain preconditioner.

linear system solution, for both solvers. The first time step is by far the most expensive, as the ILU factorizations are carried out at this stage. Thus, in Table 2 and 3 we give the execution time of the first time step, the average execution time over the remaining time steps (499 for Luo-Rudy simulation and 99 for the Rogers-McCulloch one), and the average iteration counts in the overall simulation. Results in Table 2 refer to Rogers-McCulloch model, while results in Table 3 refer to Luo-Rudy phase I model. The iteration counts of the Monodomain preconditioner appear to be essentially insensitive to the mesh size for both ionic models. Execution time of the preconditioned system remains significantly lower than the one of the symmetric Bidomain problem (see Tab. 5.4), the differences becoming more difference when we get finer meshes. The noticeable is particularly evident in the execution time of the first

time step when the incomplete LU factorization is carried out. This feature is likely relevant when the LU factorization needs to be frequently repeated during the simulations. This is the case for instance when the movement of the cardiac tissue is included in the model.

	(CG+IfpackILU)			(MPrec)		
# nodes	1^{st} step	avg. time	# iter	1^{st} step	avg. time	# iter
12586	9.66	1.31869	22.75	2.77	0.885859	5.03
29560	25.53	4.32848	29.85	7.53	2.87768	6
62566	61.34	13.4555	37.32	18.12	7.76394	6.01
127401	137.03	40.6704	46.29	41.35	20.6259	6.01
172878	211.91	61.561	48.16	61.28	31.6269	6.02
508383	1043.32	392.806	78	295.95	181.893	7
841413	1939.73	779.183	92.56	514.2	329.209	7

Table 2
Rogers-McCulloch model: execution time (in s) and iteration counts . Columns 2-4: symmetric Bidomain with PCG. Columns 5-7: non symmetric Bidomain with Monodomain preconditioner. The execution time for the first time step has been put in evidence.

	(CG+IfpackILU)			(MPrec)		
# nodes	1^{st} step	avg. time	# iter	1^{st} step	avg. time	# iter
12586	9.27	0.659178	10.358	2.37	0.425992	3.006
29560	23.42	1.80633	11.268	5.96	1.08365	3.068
62566	53.49	4.8288	12.136	13.58	3.82078	3.972
127401	118.06	13.779	14.478	33.47	9.28469	3.992
172878	170.27	22.0005	16.076	46.55	15.4344	3.99
508383	767.96	134.46	26.894	198.45	58.1504	4.04
841413	1509.6	294.201	33.268	333.65	149.989	4.9

Table 3
Luo-Rudy phase I model: execution time (in s) and iteration counts . Columns 2-4: symmetric Bidomain with PCG. Columns 5-7: non symmetric Bidomain with Monodomain preconditioner. The execution time for the first time step has been put in evidence.

5.4 A symmetric block Gauss-Seidel preconditioner

Another block-triangular preconditioner for system (29) stems from dropping block $\mathbf{B}_{ei}$. Numerical results show that this choice is not effective. As a matter of fact, for a mesh of 29560 nodes (with the Luo-Rudy Phase I ionic model), for instance, the execution time for the first time step is 31.02s, the average iteration count is 87.114, and the average execution time is 24.4803s, showing that this choice is more expensive with respect to both the Monodomain preconditioner based on the non symmetric formulation and the ILU-CG preconditioner (see Table 3). This can be explained by observing that dropping block $\mathbf{B}_{ei}$ amounts to neglect a significant part of the Bidomain problem (29), in particular when $\Delta t \to 0$. On the other hand, in the non symmetric formulation (17) the effects of dropping block $\mathbf{B}_{ue}$ are less relevant since the neglected block has the structure of the subtraction of two terms that is made "small" for a suitable choice of the Monodomain parameter λ.

	ILU / MPrec (RMC)			ILU / MPrec (LR1)		
# nodes	1^{st} step	avg. time	# iter	1^{st} step	avg. time	# iter
12586	3.4874	1.4886	4.5229	3.9114	1.5474	3.4458
29560	3.3904	1.5042	4.9750	3.9295	1.6669	3.6728
62566	3.3852	1.7331	6.2097	3.9389	1.2638	3.0554
127401	3.3139	1.9718	7.7022	3.5273	1.4841	3.6268
172878	3.4581	1.9465	8.0000	3.6578	1.4254	4.0291
508383	3.5253	2.1595	11.1428	3.8698	2.3123	6.6569
841413	3.7723	2.3668	13.2229	4.5245	1.9615	6.7894

Table 4
Ratio of the CPU times and ratio of iteration counts between conjugate gradient method with ILU preconditioner and flexible GMRES with Monodomain preconditioner. Rogers-McCulloch model (columns 2-4) and Luo-Rudy phase I model (columns 5-7).

6 Conclusions

We introduced a preconditioner for the Bidomain problem in electrocardiology, based on a non symmetric formulation and on a suitable extension of the Monodomain model. We proved its optimality, assessed both theoretically by Fourier analysis and numerically by 3D numerical tests. The preconditioner

seems to be pretty insensitive to both the size of the system and the time interval considered. As the size of the problem increases, the better performances of Monodomain preconditioner applied to the non symmetric Bidomain with respect to ILU preconditioner applied to the symmetric Bidomain become ever more evident. No parallelism has been included in the preconditioner solution, and we expect that their adoption could provide a strong improvement in terms of CPU times.

There are some aspects that deserve to be investigated. On one hand, it is clear that parameter λ can play a relevant role in enhancing the performances of the preconditioner. A fine analysis for the definition of the optimal value of this parameter is missing at the moment. On the other hand, many medical problems could have a significant insight thanks to numerical simulation. In particular the relations between electrical and mechanical dissynchrony in the left ventricle will be investigated with this method (see Figure 5 for two screenshots from a simulation performed on a realistic ventricular geometry reconstructed from SPECT images ([3])).

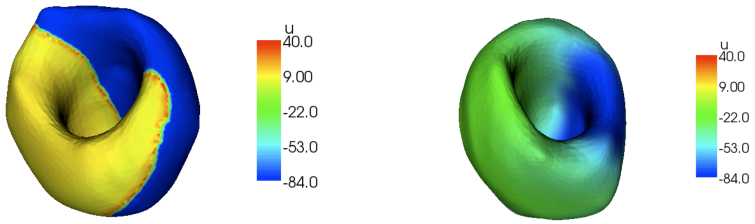

Figure 5. Screenshots of the action potential propagation at t=70ms (left) and t=400ms (right), computed on a real left ventricular geometry.

Acknowledgments The authors thank Michele Benzi (Emory University) for many fruitful discussions and suggestions in preparing this work. Fabio Nobile and Alessandro Veneziani is supported by the INDAM Project "Mathematical and Numerical Modelling of the Electro-Fluid-Mechanics of the Heart". Fabio Nobile was partially supported by Italian project PRIN 2005 "Numerical Modeling for Scientific Computing and Advanced Applications".

References

[1] `LifeV` *software*, http://www.LifeV.org.

[2] `Trilinos` *software*, http://trilinos.sandia.gov.

[3] N. Ajmone Marsan, M. Henneman, J. Chen, C. Ypenburg, P. Dibbets, S. Ghio, G. Bleeker, M. Stokkel, E. E. van der Wall, L. Tavazzi,

E. Garcia, and J. Bax, *Left ventricular dyssyncrony assessed by two three-dimensional imaging modalities: phase analysis of gated myocardial perfusion SPECT and tri-plane tissue Doppler imaging*, Eur. J. Nucl. Med. Mol. Imaging, 35 (2008), pp. 166–173.

[4] A. Alonso-Rodriguez and L. Gerardo-Giorda, *New non-overlapping domain decomposition methods for the time-harmonic Maxwell system*, SIAM J. Sci. Comp., 28(1) (2006), pp. 102–122.

[5] G. Beeler and H. Reuter, *Reconstruction of the action potential of ventricular myocardial fibres*, Journal of Physiology, 268 (1977), pp. 177–210.

[6] J. Chen, E. V. Garcia, R. Folks, C. Cooke, T. Faber, E. Tauxe, and A. Iskandrian, *Onset of left ventricular mechanical contraction as determined by phase analysis of ECG-gated myocardial perfusion SPECT imaging: development of a diagnostic tool for assessment of cardiac mechanical dyssyncrony*, J. Nucl. Cardiol., 12 (2005), pp. 687–695.

[7] J. Clements, J. Nenonen, P. Li, and M.Horacek, *Activation dynamics in anisotropic cardiac tissue via decoupling*, Ann. Biomed. Eng., 32 (2004), pp. 984–990.

[8] P. Colli Franzone, L. Guerri, M. Pennacchio, and B. Taccardi, *Spread of excitation in 3-d models of the anisotropic cardiac tissue. iii: Effects of ventricular geometry and fiber structure on the potential distribution*, Math. Biosc., 151 (1998), pp. 51–98.

[9] P. Colli Franzone and L. F. Pavarino, *A parallel solver for reaction-diffusion systems in computational electrocardiology*, Mathematical models and methods in applied sciences, 14 (2004), pp. 883–911.

[10] P. Colli Franzone, L. F. Pavarino, and B. Taccardi, *Simulating patterns of excitation, repolarization and action potential duration with cardiac Bidomain and Monodomain models*, Math. Biosc., 197 (2005), pp. 35–66.

[11] P. Colli Franzone and G. Savarè, *Degenerate evolution systems modeling the cardiac electric field at micro and macroscopic level*, in Evolution equations semigroups and functional analysis, A. Lorenzi and B. Ruffa, eds., 2002, pp. 218–240.

[12] R. FitzHugh, *Impulses and physiological states in theoretical models of nerve membrane*, Biophys. J., 1 (1961), pp. 445–466.

[13] L. Gerardo-Giorda, P. Le Tallec, and F. Nataf, *A Robin-Robin preconditioner for advection-diffusion equations with discontinuous coefficients*, Comp. Meth. Appl. Mech. Engng, 193 (2004), pp. 745–764.

[14] C. Henriquez, *Simulating the electrical behavior of cardiac tissue using the bidomain model*, Crit. Rev. Biomed. Engrg., 21 (1993), pp. 1–77.

[15] J. P. Keener, *Direct activation and defibrillation of cardiac tissue*, J. Theor. Biol., 178 (1996), pp. 313–324.

[16] J. Le Grice, B. Smaill, and P. Hunter, *Laminar structure of the heart: a mathematical model*, Am. J. Physiol., 272 (Heart Circ. Physiol.) (1995), pp. H2466–H2476.

[17] L. Luo and Y. Rudy, *A model of the ventricular cardiac action potential: depolarization, repolarization and their interaction*, Circulation Research, 68 (1991).

[18] B. F. Nielsen, T. S. Ruud, G. T. Lines, and A. Tveito, *Optimal monodomain approximation of the bidomain equations*, Appl. Math. Comp., 184 (2007), pp. 276–290.

[19] M. Pennacchio and V. Simoncini, *Efficient algebraic solution of rection-diffusion systems for the cardiac excitation process*, J. Comput. Appl. Math., 145 (2002), pp. 49–70.

[20] J. Rogers and A. McCulloch, *A collocation-Galerkin finite element model of cardiac action potential propagation*, IEEE Transactions on Biomedical Engineering, 41 (1994), pp. 743–757.

[21] B. Roth, *Action potential propagation in a thick strand of cardiac muscle*, Circ. Res., 68 (1991), pp. 162–173.

[22] Y. Saad, *Iterative Methods for Sparse Linear Systems*, PWS, Boston, 1996.

[23] S. Sanfelici, *Convergence of the Galerkin approximation of a degenerate evolution problem in electrocardiology*, Numerical Methods for Partial Differential Equations, 18 (2002), pp. 218–240.

[24] S. Scacchi and L. F. Pavarino, *Multilevel Schwarz and Multigrid preconditioners for the Bidomain system*, in Domain Decomposition Methods in Science and Engineering (Proceedings of the DD17 Conference), Springer-Verlag, 2007, pp. 631–638.

[25] E. J. Vigmond, F. Aguel, and N. A. Trayanova, *Computational techniques for solving the bidomain equations in three dimensions*, IEEE Trans. Biomed. Eng., 49 (2002), pp. 1260–1269.

[26] R. Weber dos Santos, G. Planck, S. Bauer, and E. Vigmond, *Parallel multigrid preconditioner for the cardiac bidomain model*, IEEE Trans. Biomed. Eng., 51 (2004), pp. 1960–1968.

[27] R. L. Winslow, J. J. Rice, S. Jafri, E. Marban, and B. O'Rourke, *Mechanisms of altered excitation-contraction coupling in canine tachycardia-induced heart failure, ii: model studies*, Circulation Research, 84 (1999), pp. 571–586.